RESEARCH ARTICLE

A hybrid regional climate downscaling for the southern Brazil coastal region

Danilo Couto de Souza[1] | Renato Ramos da Silva[1] | Paula Gomes da Silva[2] | Antonio Fernando Härter Fetter Filho[3] | Fernando Javier Mendez[4] | David Werth[5]

[1]Climate and Meteorology Laboratory, Department of Physics, Federal University of Santa Catarina, Florianópolis, Brazil

[2]Coastal Oceanography Laboratory, Special Coordination for Oceanography, Federal University of Santa Catarina, Florianópolis, Brazil

[3]Physical Oceanography Laboratory, Special Coordination for Oceanography, Federal University of Santa Catarina, Florianópolis, Brazil

[4]Geomatics and Ocean Engineering Group, Departamento de Ciencias y Técnicas del Agua y del Medio Ambiente, E.T.S.I.C.C.P. Universidad de Cantabria, Santander, Spain

[5]Savannah River National Laboratory, Aiken, South Carolina, USA

Correspondence
Danilo Couto de Souza, Rua Engenheiro Agronômico Andrei Cristian Ferreira s/n, Trindade, Florianópolis, SC 88040, Brazil.
Email: danilo.oceano@gmail.com

Funding information
Coordenação de Aperfeiçoamento de Pessoal de Nível Superior, Grant/Award Number: 88881146046201701; Ministerio de Ciencia e Innovación, Grant/Award Number: PID2019-107053RB-I00

Abstract

A hybrid method is applied to generate a high-resolution regional downscaling of atmospheric conditions to the southern coast of Brazil. The method consists of applying a principal component analysis to daily fields of the sea level pressure (SLP) data from the NCEP-CFSR reanalysis. A cluster analysis (K-means) is then applied to the 87 principal components that explained 95% of the variance of the time series. Daily atmospheric conditions were clustered into 36 weather types which represent the most predominant conditions observed in the study area. The estimated weather types were able to represent the major atmospheric systems affecting local climate, including the cyclones and anticyclones that are usually present in this region. Then, we applied the numerical Ocean-Land-Atmosphere Model (OLAM) to dynamically downscale the atmospheric condition that is closest to the centroid of each cluster. The model was set with a global grid and a refining approach with 6 km grid spacing over the coastal region of south Brazil. This approach allowed us to represent simultaneously the planetary waves and the local mesoscale systems, and their mutual interactions. The results provided new high-resolution atmospheric fields for the coastal region and showed that the model was capable of resolving the major local mesoscale features. The main advantage of applying such a method is in reducing the number of numerical simulations (lower computational cost) at the same time it represents the totality of the atmospheric conditions observed in the study area. The final results consist in detailed information of the local climate that can be related to injuries to the coastal area and thus is useful to support decision-makers.

KEYWORDS
circulation patterns, climate, downscaling, numerical modelling, south Brazil, weather types

1 | INTRODUCTION

Current state-of-the-art global climate models are capable of reproducing the mean large-scale climate features (Lee *et al.*, 2013; Sillmann *et al.*, 2013; Tian *et al.*, 2013).

However, the horizontal grid resolution adopted by those models does not fully represent regional features such as the effects of complex coastlines, heterogeneous topography and land use mosaics over urban and rural areas. As a result, in most cases, local circulation

patterns that affect regional climate are not properly represented.

The coastal region of south Brazil is an example of area with a complex mosaic of surfaces and sea-land interface, as it contains large estuaries, open beaches, narrow coastal plains, islands, inlets and also the most extensive lagoon system in South America (Short and Klein, 2016). However, most present-day regional climate simulations over South America use grid resolutions ranging from 40 to 80 km (Ambrizzi et al., 2019). Therefore, local communities and policy makers need climate information at finer scales than currently available.

In order to properly simulate regional climate and provide information at finer scales, modellers use a downscaling methodology, which is primarily carried out using two distinct approaches: a dynamical downscaling or statistical downscaling. The former consists of using high-resolution regional climate models (RCMs) forced by global climate models (Mearns et al., 2004; Giorgi and Gutowski, 2015). For instance, the Coordinated Regional Climate Downscaling project applies regional models to a limited area to particular regions to produce regional projections using spatial grid cells reaching 25 km (Giorgi and Gutowski, 2015). The use of numerical models in dynamical methods allows the investigation of the underlying physics of a given climate response such as interaction between distinct variables. However, long-term high-resolution RCM runs often require a large computational effort. The statistical downscaling assumes an empirical relationship between local climate variables and large-scale predictors from global models (Wilby et al., 2004). The obvious advantage of using the statistical approach over the dynamic one is the reduced computational demand. Given the nonstationary nature of the earth climate system, however, there is some concern whether statistical relationships can provide accurately projections of future climate (Wilby and Wigley, 1997).

An alternative to provide robust climate representation with low computational cost is the hybrid downscaling approach, which combines both dynamic and statistical techniques. Applications of this method include further downscaling of regional models output using statistical methods (Pryor and Barthelmie, 2014), statistical models that "mimic" the dynamical downscaling (Sun et al., 2015; Walton et al., 2015), statistical bias correction of global climate models' output which are downscaled by regional models (Colette et al., 2012) and the use of statistical analyses to select representative cases (weather types) of the regional climate and, then, dynamically downscaling them (Camus et al., 2011). The latter is an adaptation of the circulation pattern methodology for studying regional climate where atmospheric information is disaggregated into representative states (Huth, 2001; Huth et al., 2008). This methodology has been widely used for distinct finalities (e.g., Hay et al., 1991; Sheridan, 2002; Trigo et al., 2016) and is especially useful for climate change studies through the analysis of changes in the patterns of a given region over time (Huth, 2000). For South America, the studies using circulation pattern approaches are mainly focused on the central-southern portion of the continent and applications for crop producing regions of Argentina (Compagnucci and Salles, 1997; Bischoff and Vargas, 2003; Müller et al., 2003; Solman and Menéndez, 2003; Bettolli et al., 2010) or even in cold surges propagating from subtropical South America to the Amazon basin (Espinoza et al., 2013).

The framework of disaggregating atmospheric circulation patterns into weather types (Camus et al., 2011) has been used mainly in order to downscale wave climate (Camus et al., 2011; 2014; 2016; Rueda et al., 2019), extreme wave height sea conditions (Rueda et al., 2016a; 2016b) and coastal flooding and storm surge events (Rueda et al., 2016b; 2019). Although those authors selected weather types based on sea level pressure (SLP) fields, those were only used to downscale maritime variables such as wave height and the water level. This framework has yet to be applied for downscaling local climate variables.

In the present study, we applied a methodology based on the approach of Camus et al. (2014). We used a hybrid downscaling methodology to select and simulate 36 weather types, which represent the totality of the local climate conditions. Here, we dynamically downscaled those cases using high-resolution regional grids in the ocean land atmosphere model (OLAM; Walko and Avissar, 2008a). The application of such methodology allows the identification of the major weather patterns acting over the study region, while the high-resolution grids guaranteed the representation of phenomena ranging from large-scale to local-scale circulation. Finally, we analyse the low-level atmospheric circulation related to the weather types and discuss applicability of the proposed methodology. This kind of methodology is particularly useful to reduce the computational cost and time of long-term simulations. For example, by running a few representative atmospheric conditions with the numerical model, we are able to stablish a site-specific statistical relationship between input and output variables. After that, the statistical model can be applied to simulate, with very low computational cost, the time series of climate hindcast, forecast and even projections. The downscaling of climate projections is, for instance, the goal of the Regional Oceanic and Atmospheric Downscaling with the Brazilian Earth System Model project (ROAD-BESM; https://road-besm.ufsc.br).

2 | METHODOLOGY

2.1 | Atmospheric circulation in the study area

The southern region of Brazil (SBr) comprises the states of Paraná, Santa Catarina and Rio Grande do Sul states (Figure 1a). The climate of the coastal SBr is strongly influenced by the presence of the South Atlantic Subtropical Anticyclone (SASA), a high-pressure system resulting from the subsidence side of the Hadley Cell (Garreaud et al., 2009), which brings moisture and warm advection to the region. Due to the SASA, the prevailing winds are northeasterly in SBr coast and the day-to-day variability is correlated with changes of its position and to the cold air incursions on the region.

The mesoscale atmospheric conditions that affect the weather in the SBr are modulated by the passage of mid-latitude baroclinic waves, related to the occurrence of low-level high-/low-pressure systems through the region. The low-level geostrophic flow resulting from a cyclone over the ocean and an anticyclone over the continent is responsible to cold air incursions over southeast South America (Compagnucci and Salles, 1997; Garreaud, 2000). Those cold air incursions are the leading mode of variability in most areas of subtropical South America (Garreaud, 2000). During winter, those air incursions can trigger freeze events in the southern and southeastern Brazil, causing impacts to crop production (Seluchi and Marengo, 2000; Marengo et al., 2002).

Almost one third of the SBr annual precipitation is related to extratropical cyclones over the western South Atlantic Ocean (SAO; Reboita et al., 2018). The cloudiness and strong winds often associated with those systems also influence local weather. These extratropical cyclones can induce high ocean waves and cause the elevation of the water table, which triggers beach erosion episodes in SBr, strongly affecting local coastal

communities (Parise et al., 2009; Machado et al., 2010; Parise and Farina, 2012; Guimarães et al., 2014; Gomes da Silva et al., 2016; Albuquerque et al., 2018).

Another important feature of the regional climate is the South American Low Level Jet which transports moisture from the Amazon basin to the southeast South America (Seluchi and Marengo, 2000; Salio, 2002; Seluchi et al., 2003; Marengo et al., 2004). This jet is related to development of mesoscale convective systems over the region (Salio et al., 2007) and corresponds to 20–40% of summer precipitation (Salio, 2002).

The SBr has a complex land cover. It presents a variable topography, a very heterogenic vegetation surface and a complex coastal interface with the Atlantic Ocean (Figure 1b). This complex surface has an important influence on the mesoscale atmospheric circulations such as the local breezes. Thus, in order to represent the major mesoscale features relevant for the climate of the study area, high-resolution data from atmospheric models are required.

2.2 | Weather type classification

The methodology applied here is summarized in Figure 2. The processes used for defining the weather types (WT) for the coastal region of southern Brazil followed the framework described by Camus et al. (2014). Such methodology has been applied to explain the weather types acting over several coasts of the world and shown to be an efficient way to describe the main synoptic patterns in these areas: for example, Rueda et al. (2019) and Cagigal et al. (2020), in New Zealand; Antolínez et al. (2018) and Anderson et al. (2019), in the United States; and De Leo et al. (2020), in Italy. The distinct weather patterns were identified using daily mean sea level pressure (SLP) and SLP gradient fields from the National Center for Environmental Protection (NCEP)
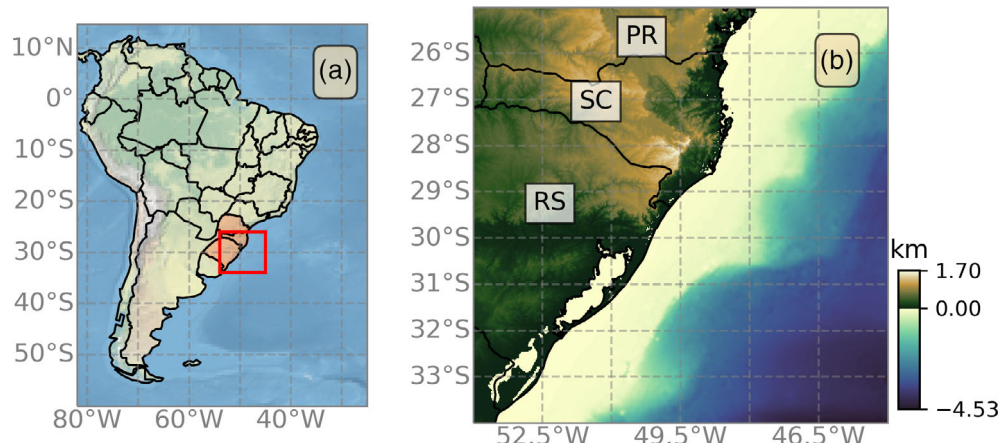
FIGURE 1 (a) South America topography indicating the study area and (b) southern Brazil and coastal area of Paraná (PR), Santa Catarina (SC) and Rio Grande do Sul (RS) states [Colour figure can be viewed at wileyonlinelibrary.com]
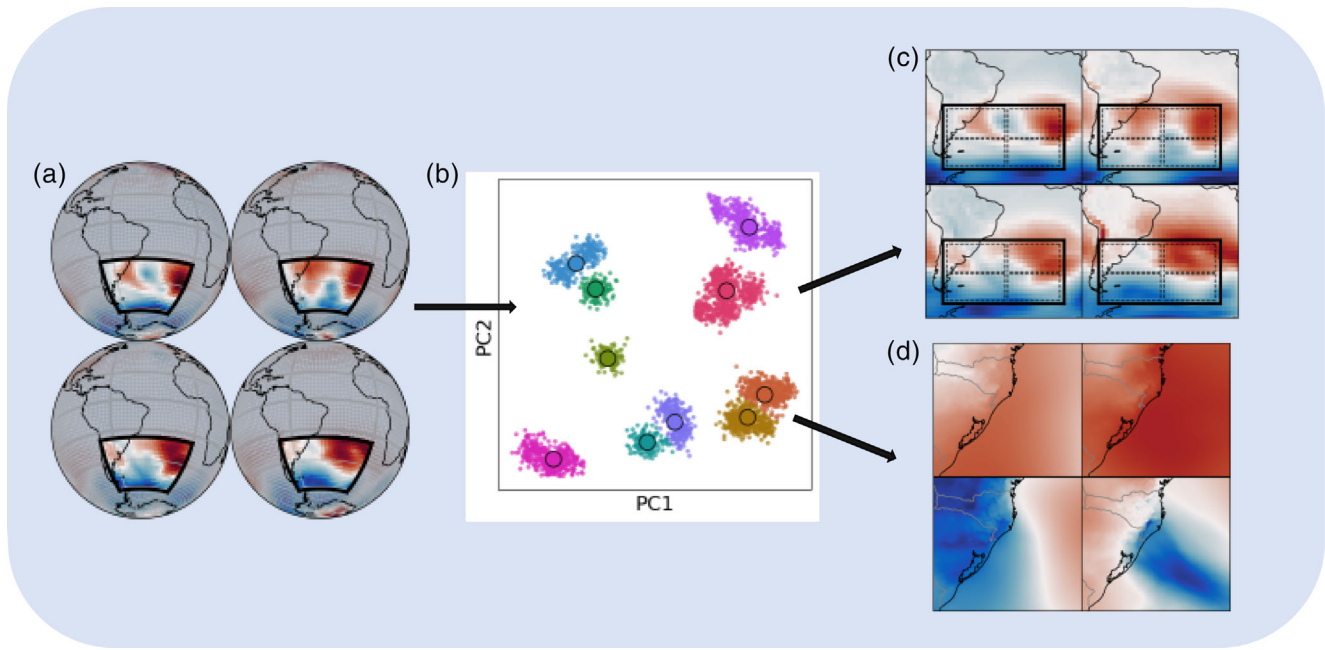
FIGURE 2 Methodological flowchart. (a) Low-resolution GCM input and domain selected for the SLP analysis. (b) Demonstration of the weather types selection with the *K*-mean clustering method. Each small coloured point represents a distinct event, while the bigger points represent the centroid of each cluster determined by the algorithm. The axis represents only the first and second principal components for clarity. (c) Analysis of synoptic patterns related to each weather type. The domain was further divided in subdomains for the surface conditions classification (Table 1). (d) High-resolution domain centred in the coastal area of SBr (Figure 1) used for the dynamical downscaling [Colour figure can be viewed at wileyonlinelibrary.com]

Climate Forecast System Reanalysis (CFSR) with 1° horizontal resolution (Saha *et al.*, 2014). The time period used included data from 1979 to 2010.

The bounding box used to define the WT was 62°–25°S latitude and 70°W to the 0° longitude (Figure 2a). As we intend further to use the generated data as input for hydrodynamic models, in order to define this domain, we did as follow: first, it was determined the area of influence of energy fluxes from wave propagation to the interest area (SBr). This was performed by the use of the ESTELA (Evaluating the Source and Travel-time of the wave Energy reaching a Local Area) methodology (Pérez *et al.*, 2014). Then, the domain was adjusted to encompass the generation area determined by the ESTELA as taking 6 days to reach SBr, which is the generation area related to most wave energy that reaches SBr (not shown). Finally, the SLP over the continent was removed as it does not directly influence the hydrodynamic conditions.

A principal component analysis was applied to the time series of SLP fields to reduce the dimensional space of the dataset (Figure 3). The synoptic conditions associated with the four main components can be explained as follows: PC1 is associated with either a large-scale cyclone or an anticyclone located at approximately 47°S, 35°W. PC2 is related to a cyclonic (anticyclonic) system near the southern part of South America, at approximately 55°S, 50°W, associated with a high-pressure (low-pressure) system northeast, at approximately 40°S, 10°W. In PC3 there is an anticyclone (cyclone) near Uruguay/SBr at approximately 40°S, 55°W, and a cyclone (anticyclone) at approximately 55°S, 15°W. Lastly, PC4 is associated with an anticyclone (cyclone), at approximately 37°S, 37°W, and two cyclones (anticyclones) both at southwest and east from it, at approximately at 57°S, 60°W and 35°S, 5°W, respectively. Somewhat similar results were found by Compagnucci and Salles (1997), although the authors used SLP data from continental stations to construct EOF maps.

The four PCs in Figure 3 explain only about 40% of the variance of the dataset. Here, we are interested on representing the majority of the atmospheric conditions, including those that result from the combination of PCs not represented by the main four. Therefore, a larger number of PCs were considered in our analysis. A *K*-means technique was applied to the 87 PCs, which explain 95% of the variance, to cluster the data into 36 weather types (Figure 2b). Each daily atmospheric condition represents a linear combination of PCs, and the cluster analysis reveals groups of days with similar combinations of PCs. The number of clusters (*N*) is predetermined by the user and must guarantee the higher
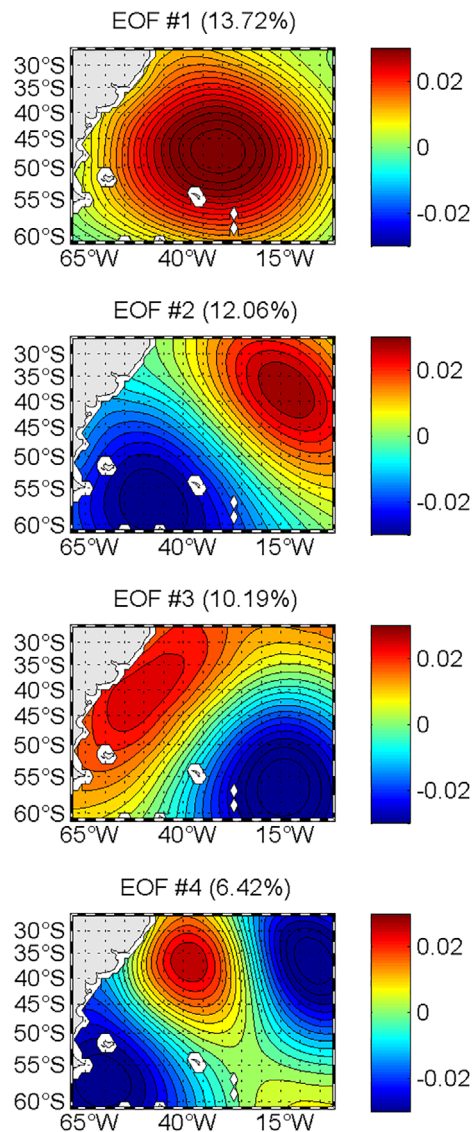
FIGURE 3 The first four EOFs for the study area, explaining approximately 40% of the total variance [Colour figure can be viewed at wileyonlinelibrary.com]

variability between clusters and the lower variability within each cluster. A sensitivity analysis (not shown) was carried out with different N (from 16 to 100) and N equals to 36 showed the best results. Each daily atmospheric condition was attributed to one of the 36 weather types which are graphically represented by the centroid of each cluster. This graphic representation allows to easily check the main atmospheric features in the study area.

2.3 | Cases selected for simulation

Once the clusters were defined, we can assume that each data point is well represented by its respective weather type (i.e., the centroid of each group in the PC space). The cases selected for the dynamical downscaling with the OLAM model were those positioned closest to the centroid. By doing the selection according to the WT, we guarantee the representation of all existent weather patterns in the downscaling. Besides, by using the weather condition that is closest to the centroid, we ensure that each group is well represented.

However, 4 out of those 36 WT (WTs 02, 06, 25 and 27) corresponded predominantly to time periods previous to 1981, with unsatisfactory data homogeneity for the Southern Hemisphere (Sterl, 2004). For those cases, we used then the dates closest to the WT centroid that represented time periods more after 1981. Those were the second, fourth, third and third case closest to the centroid, respectively.

2.4 | Numerical model description and dynamical downscaling experimental design

The OLAM model computing structure and parameterizations were built upon the Regional Atmospheric Modeling System (RAMS; Walko and Avissar, 2008a; 2008b). The main advantage of this model is that it allows the use of a global computational grid with a refined resolution approach for regions of interest. The use of a global domain with high-resolution regional grids with a two-way communication between them makes the OLAM model very versatile with many possibilities for numerical studies.

The OLAM resolves the Navier–Stokes equations through a finite-volume method (Walko and Avissar, 2008a; 2008b). The mass and momentum fields coupling of grid elements are made though an Arakawa-C scheme (Wenneker *et al.*, 2002) and the adjustment to the topography follows the shaved grid scheme (Adcroft *et al.*, 1997). The grid elements are nonstructured hexagons that can be further divided in order to increase horizontal resolution.

For the current study we adopted a model grid set up with the global horizontal resolution of about 200 km. The grid spacing is progressively reduced up to approximately 6 km in the southern Brazil (Figure 4). This level of refinement allows representation of the regional-scale features in the ocean–land interface that may affect local weather. We adopted 49 atmospheric vertical levels with varying resolution (from 60 m in the levels closer to the surface to 2,000 m in the upper stratosphere) along a 35 km high layer.

The numerical simulations were set to last 10 days, starting 3 days prior to the selected dates (Table 1) for model spin up. This time range represents the complete
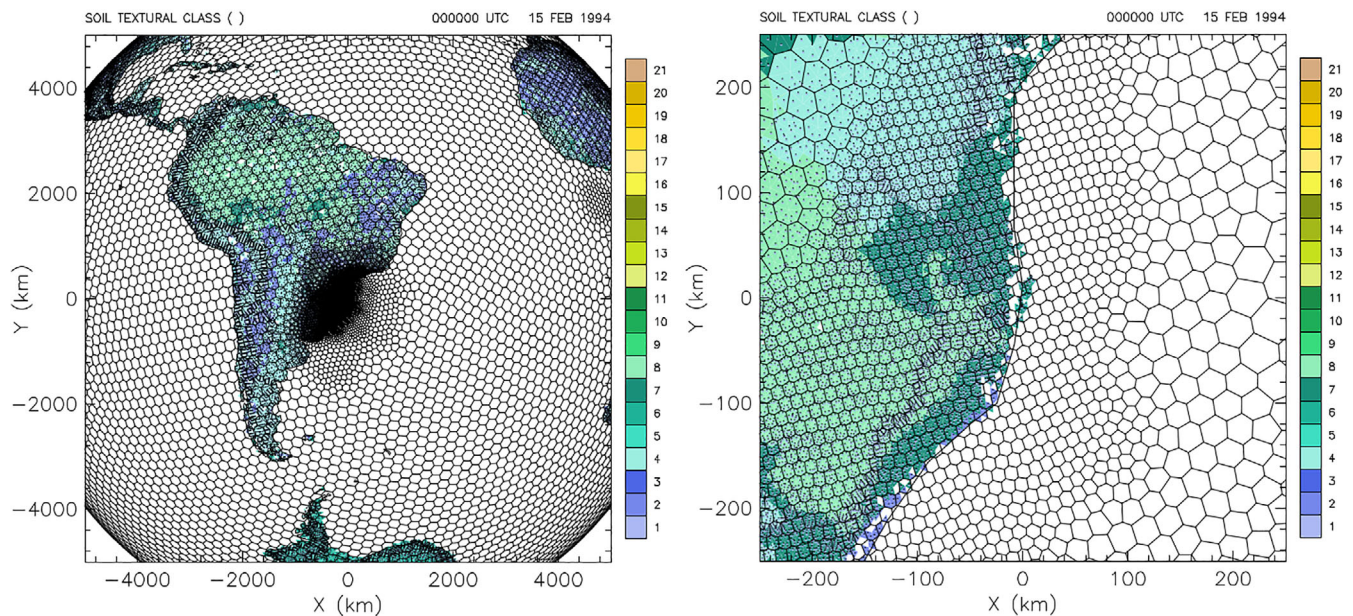
FIGURE 4 Model global grid used for the dynamical downscaling and the regional grids centred in the coastal region of southern Brazil. The contours denote distinct soil texture classes [Colour figure can be viewed at wileyonlinelibrary.com]

evolution of the major weather patterns and its further effects on near coast oceanic conditions. In order to maintain numerical stability, we adopted a 10-s time step for the simulations.

The initial atmospheric conditions were obtained from the CFSR fields. Input variables included wind fields (u and v components), geopotential height, air temperature and relative air humidity. Those variables were updated every 6 hr in the model for a light nudging on the coarser grid. Input oceanic condition consisted in the Optimum Interpolation Sea Surface Temperature (OISST) from the National Oceanic and Atmospheric Administration (NOAA), which was weekly updated (Reynolds *et al.*, 2002; 2007).

The physical parameterizations adopted included a cumulus convection parameterization (Grell and Freitas, 2014), the diffusion coefficient for atmospheric fluxes parameterization (Smagorinsky, 1963), the cloud microphysics parameterization (Walko *et al.*, 1995; Meyers *et al.*, 1997) and the short- and long-wave radiation parameterization (Mlawer *et al.*, 1997). Turbulent fluxes related to soil and vegetation cover were calculated through the use of a submodel, the Land Ecosystem-Atmosphere Feedback Model (LEAF-3; Walko *et al.*, 2000).

The OLAM model was previously validated using the same configurations as adopted here but for 12 extreme events that affected the southern coast of Brazil (de Souza and Ramos da Silva, 2021). Despite a maximum bias of 2 hPa and a negative bias for precipitation, the dynamical downscaling of CFSR fields using the

OLAM presented great agreement with observation and reanalysis data in simulating the temperature, wind and SLP fields for the selected events. Therefore, the dynamical downscaling proposed here is suitable for representing the main synoptic systems that affect the weather in south Brazil.

2.5 | Data used for the model validation

In order to verify if the OLAM was capable of accurately downscale the CFSR atmospheric fields, we compared it results with land meteorological stations. We used the stations from the Brazilian National Institute of Meteorology (INMET), freely available at https://bdmep.inmet. gov.br. For this validation, we used all stations available for the study area (Figure 1).

For the model comparison with the observations, we accessed the classic metrics such bias, mean average error (MAE), root of the mean squared error (RMSE), mean squared error (MSE) and the Pearson's correlation index (ρ). Additionally, the MSE was divided into de dissipative and dispersive components (MSE_{diss} and MSE_{disp}), which indicate phase errors and errors associated with intensity of the given atmospheric field, respectively, and we also accessed the ratio between simulated and observed standard deviation (σ_s/σ_o), where a number closer to 1 indicates better model results (Hallak and Pereira Filho, 2011). All metrics and analysis performed here are described in Taylor (2001), Hallak and Pereira Filho (2011) and de Souza and Ramos da Silva (2021).

TABLE 1 Dates (defined as the day closest to each cluster centroid), synoptic conditions related to each weather type (WT) and wind direction in the coastal SBr

No.	Dates	Surface conditions	Wind	No.	Dates	Surface conditions	Wind
01	2000-05-21	NW-AC/NE-CS	E/NE/N	19	1987-07-01	NE-AC/SE-CS	NW/SE
02	1995-04-14	NW-AC/NE-CS/NE-AC	SW/S/SE	20	1994-02-06	NW-AC/NE-AC/SE-CS	SE
03	2004-04-05	NW-AC/SE-CS	S/E/NE	21	2002-03-04	NE-AC/SW-CS	NE/N
04	2000-10-01	AC*/SE-CS	N/NE	22	1989-09-30	NW-AC/NE-AC/SE-CS	S/NW
05	2009-01-28	NW-AC/NE-AC	NE/E	23	1999-02-15	NW-CS/NE-CS	E/NE
06	1984-09-04	AC*	E/NE/SE	24	2004-03-08	NE-AC/SE-CS	NE
07	1997-05-22	NW-C/NE-AC	W	25	1999-01-20	NW-AC/SE-CS	W/NE/E
08	2005-05-07	NW-AC/NE-AC	S/SW	26	1998-02-13	NW-AC/NE-AC	E
09	2006-10-20	NWSW-AC/SE-CS	SE/E	27	1989-08-28	NW-AC/SE-CS	SW/S
10	2004-01-07	NW-AC/SW-AC	NE	28	1990-11-30	NW-C/NE-AC/SE-AC	E/NE
11	1982-10-01	NWSW-AC	NE	29	2005-11-29	NE-AC/SW-CS	NE/E
12	1998-10-04	SW-CS/NE-AC	N/NE	30	2003-11-30	NE-AC/SE-CS	E/NE
13	1986-05-03	SW-CS	SE	31	1983-09-18	NW-AC/NE-CS/SW-CS	E/NE/SW
14	2004-02-06	NW-AC/SE-CS	S/SE	32	2010-05-04	NE-AC/SW-CS/SE-CS	N/W/S
15	2005-02-24	NW-AC/NE-AC	E/NE	33	1999-09-27	NW-AC/SE-CS	SW/SE
16	1986-12-02	NE-AC/SE-CS	SW/NE/NW	34	1998-08-15	NE-AC/SW-CS/SE-CS	N/S
17	1998-12-28	NE-AC/SE-CS	NE	35	1986-03-15	NE-AC/SW-CS	S/E
18	1983-03-08	NE-AC	W/NE	36	1994-01-14	SW-CS/SE-CS	NE

Note: More than one direction indicates that it varies along the PR, SC and RS coastlines, respectively. Surface conditions acronyms are designed accordingly to the position of the prevailing cyclonic (CS)/anticyclonic (AC) features in the subdomain of SLP analysis (Figure 2). *Anticyclonic pattern across most of the domain.

3 | RESULTS

3.1 | Weather types in southern Brazil

Figure 5 shows the 36 WTs obtained from the statistical analysis with the SLP fields. All WTs comprise transient high- and low-pressure systems in the study area or the adjacent oceanic region. The dates corresponding to the 36 selected cases (those closest to their respective centroids) and the surface synoptic conditions for the simulated cases are presented in Table 1. The synoptic conditions presented at Table 1 do not exactly match the conditions (SLP and wind fields) seen in Figure 5 (see also Figure 6) as the latter represents the CFSR data cluster centroids, while the former represent the downscaled simulated fields for the cases closest to the centroids.

For the analysis of synoptic conditions associated with the 36 selected cases (Table 1), we analysed the position of cyclonic/anticyclonic systems in respect to subdomains of the original SLP fields (see left panel in Figure 2 and S1, Supporting Information). In most of the cases there was an anticyclone (AC) located in central SAO (South Atlantic Ocean—NE of the domain). This pattern occurs in 23 of all WT (02, 05, 07, 08, 12, 15 to 24, 26, 28 to 32, 34 and 35) and represents the cases when the SASA

was present. The second most prevailing condition was a cyclonic system (CS) in southern SAO (SE of the domain), occurring in 17 of the cases (WTs 03, 04, 09, 14, 16, 17, 19, 20, 22, 24, 25, 27, 30,32 to 34 and 36). Another frequent feature was the AC positioned closer to the continent (NW of the domain), mostly associated with a post frontal anticyclone with the CS located in the central part of the SAO (SW of the domain—related to cyclogenesis close to the SBr region prior to the event). Least common were the occurrence of a CS close to the Brazilian coast (SW of the domain) and in the central SAO (SE of the domain).

From the results, it is possible to see that, for most cases (WTs 03, 04, 09, 10, 12 14, 16, 17, 19 to 22, 24, 25 and 27 to 35), there was an AC in either or both NE/NW of the domain in association with a CS in either or both SE/SW of the domain. Those patterns correspond to the position of the SASA (or a postfrontal AC moving towards the SASA climatological position) and a CS moving from the southern part of South America towards the Southern Ocean. Another frequent pattern observed was an AC in the NW of the domain in association with an AC in the NE parts of the domain, without the presence of a CS. This pattern illustrates a transient (postfrontal) AC before merging with the SASA. Other patterns can be identified, but they were less common among the WTs.
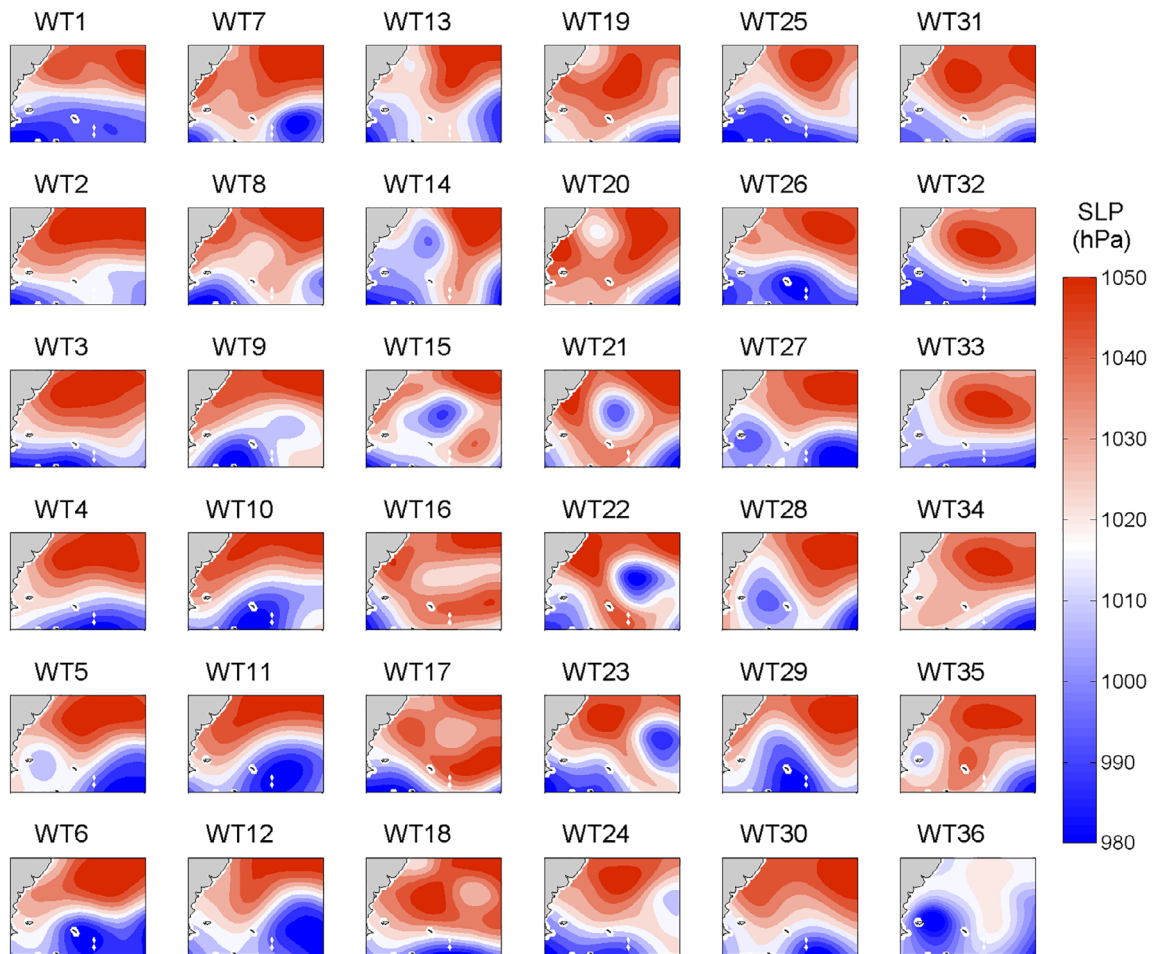
FIGURE 5 The 36 weather types selected from the statistical downscaling. The contours indicate isobars from SLP (hPa) daily mean, relative to the dates in Table 1 [Colour figure can be viewed at wileyonlinelibrary.com]

3.2 | Model validation and added value

Figure 6a shows the dynamically downscaled results from the OLAM model displaying SLP fields and wind vectors across the high-resolution domain (see also Figure S2), for each WT. Meanwhile, Figure 6b displays the same fields but for the CFSR, for comparison. It can be seen that both CFSR and OLAM represented a similar spatial pattern for the SLP, as the position of high- and low-pressure systems coincide. The OLAM and CFSR SLP field presented a very high correlation ($\rho = 0.96$, not shown). However, the high resolution presented by the OLAM model is able to capture the effects of the topography in the simulated fields, as can be seen, for example, in WT 3, 10, 12, 14, 15, 18, 27 and 31 (but also over some extent in all the presented WT). On those WT it can be seen that the SLP fields especially over the continent differ between the OLAM and the CFSR, as in the OLAM the contours represent details related to finer-scale structures such the complex topography in the SC and PR states coasts and the lagoon systems in the RS state coastal region (Figure 1).

The OLAM and CFSR SLP fields were compared with the INMET corresponding to each WT time periods available in the dataset (Figure 6c,d). Both OLAM and CFSR models, although showing small negative bias, presented a good agreement with the observations, which is further explored in the Taylor's diagram (Figure 6e) and in the statistical metrics (Table 2). The Pearson's correlation coefficient indicates very high correlation between OLAM and INMET data ($\rho = 0.9$), while the CFSR correlation was high ($\rho = 0.88$). Also, the downscaling resulted in improvements in almost every analysed metric, as it resulted in a better ratio of σ_s/σ_o and lowers MAE, MSE and RMSE. The higher MSE_{disp} than for both models indicates that the differences with the observations are more likely to be related with the positioning of the pressure fields than with the simulated intensity.

The wind speed is the atmospheric field analysed here that presented the weakest correlation between OLAM and the CFSR ($\rho = 0.54$). For most WT, the overall spatial pattern of wind speed simulated by the OLAM model matches the ones presented by the CFSR (Figure 7a,b).
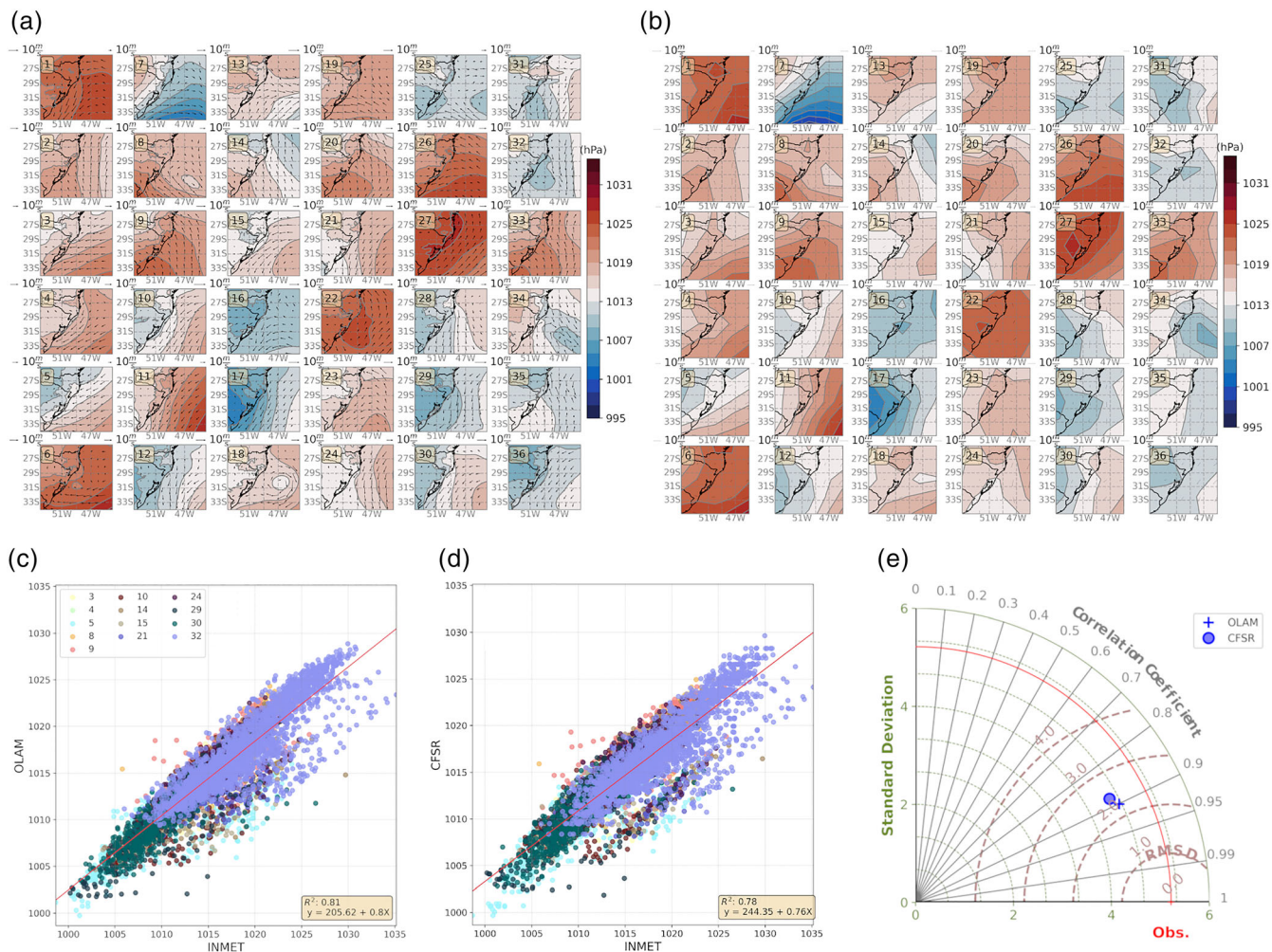
FIGURE 6   (a) OLAM model results snapshot for the selected weather types (WT) SLP (hPa) and wind field vectors at 1200 LST (GMT-3). From the first to the last WT, they are grouped from top to down and from left to the right. The color contours represent the position of low-/high-pressure systems in blue/red, respectively, while the vectors indicate the wind direction. (b) Same as in (a), but for CFSR. (c) Comparison of the OLAM SLP with the weather stations, for all WT dates which data was available. (d) Same as (c), but for comparing CFSR with the weather stations. (e) Taylor's diagram comparing OLAM and CFSR skill to represent the SLP fields, using the weather stations as reference

TABLE 2   Statistical metrics for comparing OLAM and CFSR atmospheric fields with the INMET stations data

	SLP		Wind speed		Total acc. precipitation	
	OLAM	CFSR	OLAM	CFSR	OLAM	CFSR
Average	1014	1014	3.63	4.46	26.27	50.92
Bias	−0.54	−0.27	1.04	1.87	−15.25	9.40
MAE	1.56	1.72	1.71	2.44	27.35	31.41
σ_s/σ_o	0.88	0.86	1.05	1.24	0.80	1.26
RMSE	2.33	2.47	2.22	3.08	39.48	46.80
MSE	5.45	6.12	4.94	9.47	1558.29	2189.96
MSE$_{diss}$	0.65	0.61	1.08	3.69	288.73	184.81
MSE$_{disp}$	4.79	5.52	3.86	5.78	1269.56	2005.15
ρ	0.90	0.88	0.46	0.31	0.45	0.45

Note: The metrics used were the model bias, mean average error (MAE), the ratio between simulated and observed standard deviation (σ_s/σ_o), root of the mean squared error (RMSE), mean squared error (MSE), which was divided into de dissipative and dispersive components (MSE$_{diss}$ and MSE$_{disp}$), and the Pearson's correlation index (ρ). The metrics were calculated using the data for all WT.
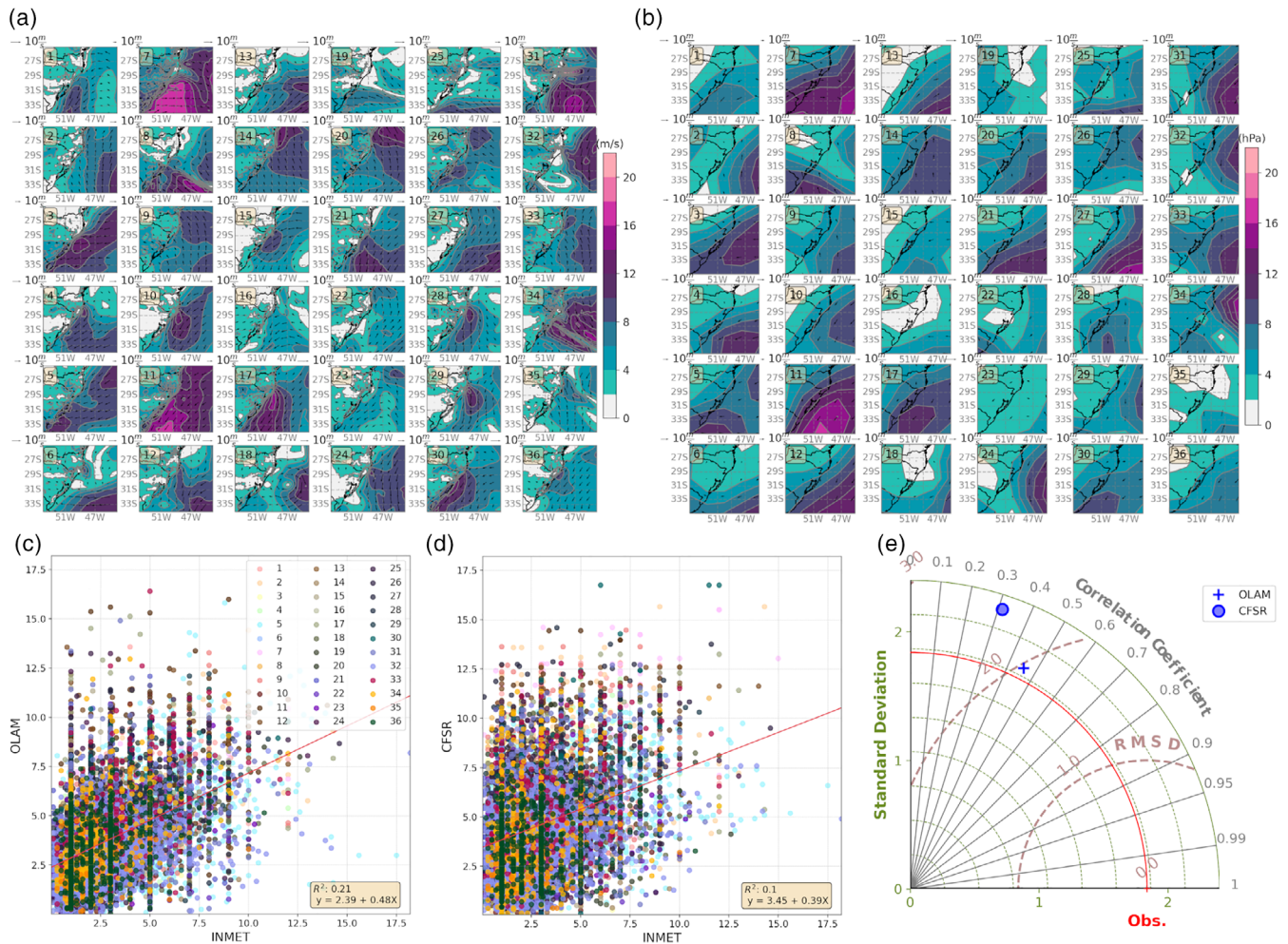
FIGURE 7 Same as Figure 6, but for wind speed

For example, the position centres of maximum and minimum velocities are similar, although there are differences in their shapes and intensities.

Compared to the station data, the CFSR presented low correlation ($\rho = 0.31$) than OLAM ($\rho = 0.46$; Table 2 and Figure 7e) for the wind speed. Besides, the downscaled fields presented improvements on all statistical metrics (Table 2). This indicates that the increased model resolution by the downscaling process leads to better representation of the wind fields and also, that the more complex spatial patterns shown in Figure 7a (when compared to Figure 7b), is related to a better representation of the finer-scale processes rather than being generated by computational modes.

For the simulated total 10 days accumulated precipitation, the OLAM and CFSR presented high correlation values ($\rho = 0.84$), although the OLAM downscaled fields often presented lower totals (Figure 8a,b). Both the OLAM and CFSR presented moderate correlation with the INMET stations data ($\rho = 0.45$, for both). Figure 8c shows that, for the WT presented here, the OLAM model overall tends to underestimate the precipitation, which is demonstrated by its negative bias (Table 2). Meanwhile, Figure 8d shows that the CFSR often overestimates the accumulated values lower than approximately 150 mm, but underestimates the values greater than this threshold, resulting in a positive bias of smaller absolute valour than the OLAM's (Table 2). However, the other metrics at Table 2 point to a better overall result by the OLAM model, as there is a reduced MAE, RMSE and MSE values and also a σ_s/σ_o ratio closer to 1.

3.3 | Downscaled atmospheric conditions

The most frequent wind direction, as downscaled by the OLAM model (Figure 6a), in all sectors of coastal SBr was northeasterly, followed by easterly (Table 1). Both are related to the SASA positioned in the middle of the SAO (northern part of the domain) or with a cyclogenesis event near the coast (for example, WT17 and 29). In
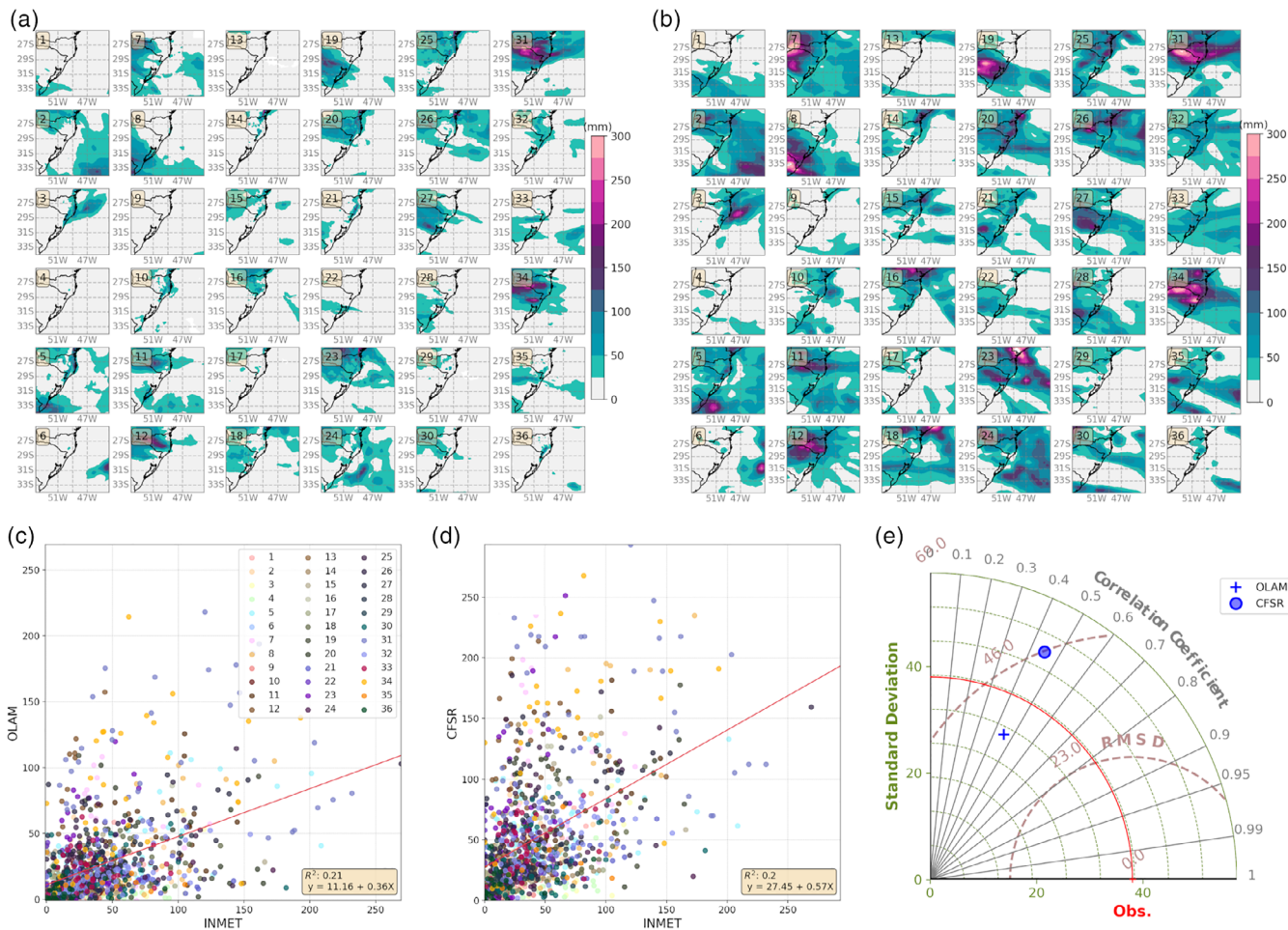
FIGURE 8   Same as Figure 6 but for the total accumulated precipitation during all 10 days of simulation

general, the position of the SASA further away from the SBr coast resulted in more northeasterly than easterly winds and moderate wind speeds (around 10 m·s^{-1}). Wind speed was often higher for RS and southern SC state coasts. In contrast, the PR state coastal area mostly presented calmer conditions, with lower wind velocities. Southerly winds were mostly associated to the position of an anticyclone close to the continent (NW of the domain—likely a postfrontal anticyclone).

Wind direction related to cyclonic systems changed accordingly with the position of the system and also along the coast. For example, in WT18 the position of the cyclone in the oceanic area close to the RS state coastline was associated with mostly easterly winds along the RS coast and southerly winds near the SC coast. The highest wind velocities (Figure 7a) were obtained from WT31, WT07 and WT11. In both WTs 31 and 07 there were cyclogenesis events near the coastal region of SBr while in WT11 there was a postfrontal anticyclone very close to SBr. In WT31 the cyclogenesis event near SBr could not be detected through the low-resolution CFSR fields (its

SLP fields do not show a closed low) but its signature can be seen in the OLAM model downscaled fields (Figures 6 and S2).

Figure 8 presents the results from OLAM for the 10 day precipitation accumulation for each WT. The results show that WT31, WT34 and WT23 had the highest amounts of precipitation for the study area (and also for the more continental parts of SBr), each WT representing an episode of high precipitation for each state, SC, RS and PR, respectively. In both WT31 and WT34, the precipitation was most likely associated with the passage of a cold front over SBr, which was related to the CS in the SW of the domain. WT23 was probably an event of orographic rain associated with warm and moist advections from the SAO.

Among the 15 events that resulted in precipitation in the SBr coast (WTs 02, 03, 05, 08, 10, 14, 18, 20, 23, 24, 25, 26, 27, 31 and 34), 12 were associated with the presence of an AC in the NW part of the domain. For those cases, this AC was most likely a post frontal anticyclone. However, in order to infer if the precipitation was related

with a frontal system or other meteorological system one would need to analyse the temporal evolution of each event, which is beyond the scope of the present study. Meanwhile, WTs 01, 04, 09, 13, 17, 22, 29 and 36 represented dry conditions for SBr.

4 | DISCUSSION

4.1 | Weather types and atmospheric circulation observed in south Brazil

The proposed weather types presented here represented those circulation patterns expected for the region, related to influences of the SASA as well as the high-frequency low-level synoptic variability: the year-around passage of transient high-/low-pressure systems through the region (Compagnucci and Salles, 1997; Garreaud and Wallace, 1998; Garreaud, 2000; Seluchi and Marengo, 2000; Garreaud and Aceituno, 2002). Meanwhile, the dynamical downscaling methodology provided high-resolution atmospheric fields that captured well the atmospheric systems ranging from local scale to mesoscale, including details that could not be seen in the low-resolution atmospheric fields from the CFSR reanalysis.

The occurrence probability analysis showed five predominant WT that affect the weather in the SBr as they sum up to more than 20% of the total occurrence probability. Meanwhile, the WTs seasonal occurrence probabilities presented an opposite behaviour between the austral summer and winter months. In general, during JJA and SON there is a higher occurrence probability for WT related to cyclonic systems closer to the SBr coast than for DJF and MAM. This behaviour can be explained by the enhanced cyclogenesis activity near Uruguay and in the southern region of South America during those months (Reboita *et al*., 2010a; Gramcianinov *et al*., 2019). The local effects of this cyclogenesis closer to the coast can be seen, for example, in WT08 where there is considerable amount of precipitation in the southernmost part of SBr (up to 150 mm in the 10 day accumulated) due to the passage of an extratropical cyclone's frontal system in the region. Both frontal systems and extratropical cyclones are the main atmospheric phenomena contributing for the precipitation in the region (Rao and Hada, 1990; Rao *et al*., 1996; Reboita *et al*., 2010b, 2018).

Although the spatial pattern of the OLAM and CFSR SLP fields presented similar features, the downscaling process allowed the OLAM to represent finer-scale structures absent in the coarser CFSR fields. SLP gradients such as those induced by topography are responsible for triggering local circulations that might affect the atmospheric conditions in the neighbouring region (Ferber

and Mass, 1990; Silva Dias and Jaschke, 1997; Lee and Kimura, 2001; Nishizawa *et al*., 2021). Also, the interaction between sea-land circulations and the topography on the coastal region of SBr are important mechanisms modulating its precipitation regimen (Berbery and Collini, 2000).

Despite the similar results for the SLP fields between OLAM and CFSR, the downscaling process resulted in improvements of the simulated wind speeds. This is in agreement with Mass *et al*. (2002), that showed that higher model resolutions result in higher statistical scores for the wind field rather than for SLP, as the increased resolution allowed a better representation of mesoscale topographic features. For the precipitation, previous studies have proposed that the added value of RCM is dependent of various factors, such the region surface features and the RCM driving fields/GCM (Falco *et al*., 2019; Solman and Blázquez, 2019).

The CFSR positive bias for the accumulated precipitation for the SBr coastal area is in agreement with Silva *et al*. (2011). In that study, the authors demonstrated that the CFSR has a higher (lower) probability of light (heavy) rainfall than the observed. The downscaling by the OLAM model achieved a reduction in the bias associated with the light rain (lower accumulated values), which demonstrates added value by OLAM regarding the CFSR inputs, although the high accumulates are still underestimated.

Overall the validation showed that the downscaling methodology proposed resulted in realistic atmospheric fields, especially for SLP, that represent well the atmospheric systems that modulate the climate over SBr. As the downscaling methodology is highly sensitive to the initial boundaries conditions, it is advisable further studies accessing this methodology, for example, with the new ERA5 Reanalysis, that showed promising results for SBr (Hersbach *et al*., 2019, 2020; de Assis Tavares *et al*., 2020; Fernandes *et al*., 2021).

One of the key characteristics of the low-level circulation related to the WTs presented here is a prevailing NE wind direction with moderate wind speeds near the coastal SB, related to the SASA position. This is consistent with results from Compagnucci and Salles (1997) who found that the synoptic circulation associated with the SASA was the leading pattern for the region and explained 50% of the variance. The passage of transient high-/low-pressure systems through the region was related to changes in wind direction to southerly winds, following the proposed mechanism of cold air incursions in the southern/southeastern parts of Brazil (Garreaud, 2000). The frontal systems associated with CS in the SAO are one of the main mechanisms associated with precipitation formation in the SBr (Reboita *et al*., 2010b), while the cold air incursions following

them are the leading mode of synoptic variability for the region (Garreaud, 2000; Garreaud *et al.*, 2009).

The obvious advantage of using this methodology that identifies circulation patterns from coarser global model for using them in a dynamic downscaling process is that it provides a comprehensive range of the predominant atmospheric conditions for the study area without the need to perform a long complete numerical climatology using a regional model. This is only possible due to the increasing number of available reanalysis projects nowadays. This method allows saving computational power that would be required in long high-resolution simulations. With increased resolutions, the model is able to better represent the atmosphere dynamics and surface boundary conditions, which in turn provide simulations with more accurate weather conditions. For instance, the dynamical simulations presented here took approximately 4.8 hr of computing time to perform 1 day of simulation, using eight CPU cores. Therefore, adopting the same model and PC configurations as here, a complete 30-year climatology would require running approximately 6 years of simulations. Therefore, the framework followed here allowed a fair representation of the region climate that can be performed on computers affordable to non-high budget projects.

4.2 | Potential applications

The probability of occurrence of the WT allows identification of prevailing conditions for the study area and potential risks associated with certain WTs. For instance, WTs 31 and 34 are associated with potential impacts for coastal SBr due to the high amounts of precipitation related to those events (although the precipitation maxima were located in the central parts of SBr). This is a matter of concern especially for the northern region of coastal SC state, where historical occurrence of flooding events have caused millions of dollars in economic losses, have displaced thousands of people and caused fatalities (Herrmann, 2006; Stevaux *et al.*, 2009).

The wind fields indicate WT31 and also WTs 07 and 11 as events of possible impact for the coastal SBr, as the high wind speeds can cause damage to housing and coastal infrastructures, trigger beach erosion episodes, impact port activities and cause risks for navigation (e.g., Innocentini and Caetano Neto, 1996; Parise *et al.*, 2009; Fuentes *et al.*, 2013). Meanwhile, the persistence of WT associated with dry conditions indicates risks for water supply and farming.

Other possible association that can be made with the WTs selected here is with extreme events occurring in

the study area. For instance, de Souza and Ramos da Silva (2021) reviewed major extreme events that occurred in the coastal SBr since 2000. In their study, the events they numbered from E06 to E12 fit into the WTs 03, 12, 03, 08, 07, 26 and 21, respectively. For those cases there is a close match between the synoptic conditions presented there, for the extreme events, and here for the WTs, except for events 07 and 12 (WTs 12 and 21). Those two last cases corresponded to the Itajaí Valley (north of SC state) flooding in 2008 and the Catarina Hurricane in 2004, the most extreme events that occurred in this region (Pezza and Simmonds, 2005; World Bank, 2016). For those two cases it is expected this difference between the WTs synoptic conditions and the actual events conditions due to increased intragroup variance. For the remaining events, the correspondence between them and the proposed WTs indicate that the methodology captures well not only the atmospheric circulation related to the region mean flow but also to the extreme events occurring there. Identifying WTs related to extreme events can aid forecasters identifying possible atmospheric conditions linked to hazards for SBr. Also, analysing the temporal evolution of the WTs associated to extreme events presented here for climate change scenarios from GCM output will be subject of a future study.

Identifying the atmospheric circulation patterns related to present weather conditions can also be useful for assessing future climate change scenarios. As the methodology used here is computationally cheaper than a full regional climate projection (as previous discussed) one can assess climate change scenarios for the region using, for example, data from the Coupled Model Intercomparison Project (CMIP) and adopt the same methodology as we used here for identifying future WTs for the region in a similar approach as applied by Camus *et al.* (2014) and Perez *et al.* (2015). This would allow a detailed analysis of the future weather patterns occurring in the region and also their relationship to potential impacts for the communities.

5 | CONCLUSION

The weather types presented here provided a comprehensive representation of the regional climate and the final downscaled high-resolution estimates can provide synoptic-scale variables that are important for the local population. In the present study, we used a statistical downscaling approach to identify the 36 main weather types acting over the coastal region of southern Brazil. Meanwhile, the dynamical downscaling carried out with the OLAM model provided high-resolution atmospheric fields for the coastal southern Brazil area. The analysis of

WTs occurrence probabilities indicated that the seasonal timescale largely modulates the WTs.

The horizontal resolutions achieved here are of approximately 6 km, which is at least 4 times higher than the ongoing CORDEX initiative (Giorgi and Gutowski, 2015) and 20 times higher than most GCM output. This allowed better representation of the SBr complex coastline and heterogeneous topography and thus, the model was able to capture well the region large-scale features as well as provide high-resolution information. The proposed methodology can also be applied to any other region by selecting WT and adapting the OLAM grid system for the interest region.

In the future, this methodology will be used to access climate change scenarios for the study region and to access the impact on surface oceanic waves, storm surges and coastal flooding. Changes in frequency and atmospheric patterns related to the WT may project the expected impacts and thus provide important data for the local decision-makers.

CONFLICT OF INTEREST
The authors declare no potential conflict of interest.

AUTHOR CONTRIBUTIONS
Danilo Couto de Souza: Conceptualization; data curation; formal analysis; investigation; software; validation; visualization; writing – original draft; writing – review and editing. **Renato Ramos da Silva:** Conceptualization; data curation; funding acquisition; investigation; resources; writing – original draft; writing – review and editing. **Paula Gomes da Silva:** Data curation; formal analysis; investigation; software; visualization; writing – original draft; writing – review and editing. **Antonio Fernando Hatter Fetter-Filho:** Conceptualization; formal analysis; funding acquisition; resources; supervision. **Fernando Javier Mendez:** Conceptualization; funding acquisition; methodology; project administration; software; supervision; writing – original draft. **David Werth:** Writing – original draft; writing – review and editing.

ORCID
Danilo Couto de Souza https://orcid.org/0000-0003-4121-7583
Renato Ramos da Silva https://orcid.org/0000-0002-3714-0870
Paula Gomes da Silva https://orcid.org/0000-0003-4766-8449
Antonio Fernando Härter Fetter Filho https://orcid.org/0000-0003-4843-8557
Fernando Javier Mendez https://orcid.org/0000-0002-5005-1100

REFERENCES
Adcroft, A., Hill, C. and Marshall, J. (1997) Representation of topography by shaved cells in a height Coordinate Ocean Model. *Monthly Weather Review*, 125(9), 2293–2315.

Albuquerque, M.d.G., Leal Alves, D.C., Espinoza, J.M.d.A., Oliveira, U.R. and Simões, R.S. (2018) Determining shoreline response to meteo-oceanographic events using remote sensing and unmanned aerial vehicle (UAV): case study in southern Brazil. *Journal of Coastal Research*, 85, 766–770. https://doi.org/10.2112/si85-154.1.

Ambrizzi, T., Reboita, M.S., da Rocha, R.P. and Llopart, M. (2019) The state of the art and fundamental aspects of regional climate modeling in South America. *Annals of the New York Academy of Sciences*, 1436(1), 98–120. https://doi.org/10.1111/nyas.13932.

Anderson, D., Rueda, A., Cagigal, L., Antolinez, J.A.A., Mendez, F.J. and Ruggiero, P. (2019) Time-varying emulator for short and long-term analysis of coastal flood hazard potential. *Journal of Geophysical Research: Oceans*, 124(12), 9209–9234. https://doi.org/10.1029/2019JC015312.

Antolínez, J.A.A., Murray, A.B., Méndez, F.J., Moore, L.J., Farley, G. and Wood, J. (2018) Downscaling changing coastlines in a changing climate: the hybrid approach. *Journal of Geophysical Research: Earth Surface*, 123(2), 229–251. https://doi.org/10.1002/2017JF004367.

Berbery, E.H. and Collini, E.A. (2000) Springtime precipitation and water vapor flux over southeastern South America. *Monthly Weather Review*, 128(5), 1328–1346. https://doi.org/10.1175/1520-0493(2000)128<1328:SPAWVF>2.0.CO;2.

Bettolli, M.L., Penalba, O.C. and Vargas, W.M. (2010) Synoptic weather types in the south of South America and their relationship to daily rainfall in the core crop-producing region in Argentina. *Australian Meteorological and Oceanographic Journal*, 60(1), 37–48. https://doi.org/10.22499/2.6001.004.

Bischoff, S.A. and Vargas, W.M. (2003) The 500 and 1,000 hPa weather circulations and their relationship with some extreme climatic conditions over southern South America. *International Journal of Climatology*, 23(5), 541–556. https://doi.org/10.1002/joc.894.

Cagigal, L., Rueda, A., Anderson, D., Ruggiero, P., Merrifield, M.A., Montaño, J., Coco, G. and Méndez, F.J. (2020) A multivariate, stochastic, climate-based wave emulator for shoreline change modelling. *Ocean Modelling*, 154, 101695. https://doi.org/10.1016/j.ocemod.2020.101695.

Camus, P., Mendez, F.J. and Medina, R. (2011) A hybrid efficient method to downscale wave climate to coastal areas. *Coastal*

Engineering, 58(9), 851–862. https://doi.org/10.1016/j.coastaleng.2011.05.007.

Camus, P., Menéndez, M., Méndez, F.J., Izaguirre, C., Espejo, A., Cánovas, V., Pérez, J., Rueda, A., Losada, I.J. and Medina, R. (2014) A weather-type statistical downscaling framework for ocean wave climate. *Journal of Geophysical Research: Oceans*, 119(11), 7389–7405. https://doi.org/10.1002/2014JC010141.

Camus, P., Rueda, A., Méndez, F.J. and Losada, I.J. (2016) An atmospheric-to-marine synoptic classification for statistical downscaling marine climate. *Ocean Dynamics*, 66(12), 1589–1601. https://doi.org/10.1007/s10236-016-1004-5.

Colette, A., Vautard, R. and Vrac, M. (2012) Regional climate downscaling with prior statistical correction of the global climate forcing. *Geophysical Research Letters*, 39(13), 13707. https://doi.org/10.1029/2012GL052258.

Compagnucci, R.H. and Salles, M.A. (1997) Surface pressure patterns during the year over southern South America. *International Journal of Climatology*, 17(6), 635–653. https://doi.org/10.1002/(SICI)1097-0088(199705)17:6<635::AID-JOC81>3.3.CO;2-2.

de Assis Tavares, L.F., Shadman, M., de Freitas Assad, L.P., Silva, C., Landau, L. and Estefen, S.F. (2020) Assessment of the offshore wind technical potential for the Brazilian southeast and south regions. *Energy*, 196, 117097. https://doi.org/10.1016/j.energy.2020.117097.

De Leo, F., Solari, S. and Besio, G. (2020) Extreme wave analysis based on atmospheric pattern classification: an application along the Italian coast. *Natural Hazards and Earth System Sciences*, 20(5), 1233–1246. https://doi.org/10.5194/nhess-20-1233-2020.

de Souza, D. and Ramos da Silva, R. (2021) Ocean-land atmosphere model (OLAM) performance for major extreme meteorological events near the coastal region of southern Brazil. *Climate Research. Inter-Research Science Center*, 84, 1–21. https://doi.org/10.3354/cr01651.

Espinoza, J.C., Ronchail, J., Lengaigne, M., Quispe, N., Silva, Y., Bettolli, M.L., Avalos, G. and Llacza, A. (2013) Revisiting wintertime cold air intrusions at the east of the Andes: propagating features from subtropical Argentina to Peruvian Amazon and relationship with large-scale circulation patterns. *Climate Dynamics*, 41(7–8), 1983–2002. https://doi.org/10.1007/s00382-012-1,639-y.

Falco, M., Carril, A.F., Menéndez, C.G., Zaninelli, P.G. and Li, L.Z.X. (2019) Assessment of CORDEX simulations over South America: added value on seasonal climatology and resolution considerations. *Climate Dynamics*, 52(7–8), 4771–4786. https://doi.org/10.1007/s00382-018-4412-z.

Ferber, G.K. and Mass, C.F. (1990) Surface pressure perturbations produced by an isolated mesoscale topographic barrier. Part II: influence on regional circulations. *Monthly Weather Review*, 118(12), 2597–2606. https://doi.org/10.1175/1520-0493(1990)118<2597:SPPPBA>2.0.CO;2.

Fernandes, I.G., Pimenta, F.M., Saavedra, O.R. and Silva, A.R. (2021) Offshore validation of ERA5 reanalysis with hub height wind observations of Brazil. In: 2021 IEEE PES Innovative Smart Grid Technologies Conference—Latin America (ISGT Latin America). pp. 1-5. https://ieeexplore.ieee.org/document/9542993

Fuentes, E.V., Bitencourt, D.P. and Fuentes, M.V. (2013) Análise da velocidade do vento e altura de onda em incidentes de naufrágio na costa brasileira entre os estados do Sergipe e do Rio Grande do Sul. *Revista Brasileira de Meteorologia*, 28(3), 257–266. https://doi.org/10.1590/S0102-77862013000300003.

Garreaud RD, Aceituno P. 2002. Atmospheric circulation over South America: mean features and variability. Veblen T Orme A and Young K *The Physical Geography of South America*. Oxford University Press: Oxford.

Garreaud, R.D. and Wallace, J.M. (1998) Summertime incursions of midlatitude air into subtropical and tropical South America. *Monthly Weather Review*, 126(10), 2713–2733. https://doi.org/10.1175/1520-0493(1998)126<2713:SIOMAI>2.0.CO;2.

Garreaud, R.D.D. (2000) Cold air incursions over subtropical South America: mean structure and dynamics. *Monthly Weather Review*, 128(7 II), 2544–2559. https://doi.org/10.1175/1520-0493(2000)128<2544:CAIOSS>2.0.CO;2.

Garreaud, R.D.D., Vuille, M., Compagnucci, R. and Marengo, J. (2009) Present-day South American climate. *Palaeogeography, Palaeoclimatology, Palaeoecology*, 281(3–4), 180–195. https://doi.org/10.1016/j.palaeo.2007.10.032.

Giorgi, F. and Gutowski, W.J. (2015) Regional dynamical downscaling and the CORDEX initiative. *Annual Review of Environment and Resources*, 40(1), 467–490. https://doi.org/10.1146/annurev-environ-102014-021217.

Gomes da Silva, P., Dalinghaus, C., González, M., Gutiérrez, O., Espejo, A., Abascal, A.J. and Klein, A.H.F. (2016) Estimating flooding level through the Brazilian coast using reanalysis data. *Journal of Coastal Research*, 75, 1092–1096. https://doi.org/10.2112/SI75-219.1.

Gramcianinov, C.B., Hodges, K.I. and Camargo, R. (2019) The properties and genesis environments of South Atlantic cyclones. *Climate Dynamics*, 53(7–8), 4115–4140. https://doi.org/10.1007/s00382-019-04778-1.

Grell, G.A. and Freitas, S.R. (2014) A scale and aerosol aware stochastic convective parameterization for weather and air quality modeling. *Atmospheric Chemistry and Physics*, 14(10), 5233–5250. https://doi.org/10.5194/acp-14-5233-2014.

Guimarães, P.V., Farina, L. and Toldo, E.E. (2014) Analysis of extreme wave events on the southern coast of Brazil. *Natural Hazards and Earth System Sciences*, 14(12), 3195–3205. https://doi.org/10.5194/nhess-14-3195-2014.

Hallak, R. and Pereira Filho, A.J. (2011) Metodologia para análise de desempenho de simulações de sistemas convectivos na região metropolitana de São Paulo com o modelo ARPS: sensibilidade a variações com os esquemas de advecção e assimilação de dados. *Revista Brasileira de Meteorologia*, 26(4), 591–608. https://doi.org/10.1590/S0102-77862011000400009.

Hay, L.E., McCabe, G.J., Wolock, D.M. and Ayers, M.A. (1991) Simulation of precipitation by weather type analysis. *Water Resources Research*, 27(4), 493–501. https://doi.org/10.1029/90WR02650.

Herrmann, M.L.P. (2006) *Atlas de Desastres Naturais do Estado de Santa Catarina*. Florianópolis: Instituto Histórico e Geográfico de Santa Catarina: GCN/UFSC, Cadernos Geográficos, https://www.ceped.ufsc.br/atlas-de-desastres-naturais-do-estado-de-santa-catarina-ceped/

Hersbach, H., Bell, B., Berrisford, P., Hirahara, S., Horányi, A., Muñoz-Sabater, J., Nicolas, J., Peubey, C., Radu, R., Schepers, D., Simmons, A., Soci, C., Abdalla, S., Abellan, X., Balsamo, G., Bechtold, P., Biavati, G., Bidlot, J., Bonavita, M.,

De Chiara, G., Dahlgren, P., Dee, D., Diamantakis, M., Dragani, R., Flemming, J., Forbes, R., Fuentes, M., Geer, A., Haimberger, L., Healy, S., Hogan, R.J., Hólm, E., Janisková, M., Keeley, S., Laloyaux, P., Lopez, P., Lupu, C., Radnoti, G., de Rosnay, P., Rozum, I., Vamborg, F., Villaume, S. and Thépaut, J.N. (2020) The ERA5 global reanalysis. *Quarterly Journal of the Royal Meteorological Society*, 146(730), 1999–2049. https://doi.org/10.1002/qj.3803.

Hersbach, H., Bell, B., Berrisford, P., Horányi, A., Sabater, J.M., Nicolas, J., Radu, R., Schepers, D., Simmons, A., Soci, C. and Dee, D. Global reanalysis: goodbye ERA-Interim, hello ERA5. ECMWF Newsletter. http://dx.doi.org/10.21957/vf291hehd7

Huth, R. (2000) A circulation classification scheme applicable in GCM studies. *Theoretical and Applied Climatology*, 67(1–2), 1–18. https://doi.org/10.1007/s007040070012.

Huth, R. (2001) Disaggregating climatic trends by classification of circulation patterns. *International Journal of Climatology*, 21(2), 135–153. https://doi.org/10.1002/joc.605.

Huth, R., Beck, C., Philipp, A., Demuzere, M., Ustrnul, Z., Cahynová, M., Kyselý, J. and Tveito, O.E. (2008) Classifications of atmospheric circulation patterns: recent advances and applications. *Annals of the New York Academy of Sciences*, 1(146), 105–152. https://doi.org/10.1196/annals.1446.019.

Innocentini, V. and Caetano Neto, E.D.S. (1996) A case study of the August 9, 1988 South Atlantic storm: numerical simulations of the wave activity. *Weather and Forecasting*, 11(1), 78–88. https://doi.org/10.1175/1520-0434(1996)011<0078:ACSOTA>2.0.CO;2.

Lee, S.-H. and Kimura, F. (2001) Comparative studies in the local circulations induced by land-use and by topography. *Boundary-Layer Meteorology*, 101(2), 157–182. https://doi.org/10.1023/A:1019219412907.

Lee, T., Waliser, D.E., Li, J.L.F., Landerer, F.W. and Gierach, M.M. (2013) Evaluation of CMIP3 and CMIP5 wind stress climatology using satellite measurements and atmospheric reanalysis products. *Journal of Climate*, 26(16), 5810–5826. https://doi.org/10.1175/JCLI-D-12-00591.1.

Machado, A.A., Calliari, L.J., Melo, E. and Klein, A.H.F. (2010) Historical assessment of extreme coastal sea state conditions in southern Brazil and their relation to erosion episodes. *Pan-American Journal of Aquatic Sciences*, 5(2), 277–286.

Marengo, J.A., Ambrizzi, T., Kiladis, G. and Liebmann, B. (2002) Upper-air wave trains over the Pacific Ocean and wintertime cold surges in tropical-subtropical South America leading to freezes in southern and southeastern Brazil. *Theoretical and Applied Climatology*, 73(3–4), 223–242. https://doi.org/10.1007/s00704-001-0669-x.

Marengo, J.A., Soares, W.R., Saulo, C. and Nicolini, M. (2004) Climatology of the low-level jet east of the Andes as derived from the NCEP-NCAR Reanalyses: characteristics and temporal variability. *Journal of Climate*, 17(12), 2261–2280. https://doi.org/10.1175/1520-0442(2004)017<2261:COTLJE>2.0.CO;2.

Mass, C.F., Ovens, D., Westrick, K. and Colle, B.A. (2002) Does increasing horizontal resolution produce more skillful forecasts? *Bulletin of the American Meteorological Society*, 83(3), 407–430. https://doi.org/10.1175/1520-0477(2002)083<0407:DIHRPM>2.3.CO;2.

Mearns, L.O., Giorgi, F., Whetton, P., Pabon, D., Hulme, M. & Lal, M. Data Distribution Centre of the Intergovernmental Panel on Climate Change, p. 38. Available at: https://www.researchgate.net/profile/Linda-Mearns/publication/251994345_Guidelines_for_Use_of_Climate_Scenarios_Developed_from_Regional_Climate_Model_Experiments/links/0deec529bad1f1656a000000/Guidelines-for-Use-of-Climate-Scenarios-Developed-from-Regional-Climate-Model-Experiments.pdf

Meyers, M.P., Walko, R.L., Harrington, J.Y. and Cotton, W.R. (1997) New RAMS cloud microphysics parameterization. Part II: the two-moment scheme. *Atmospheric Research*, 45(1), 3–39. https://doi.org/10.1016/S0169-8095(97)00018-5.

Mlawer, E.J., Taubman, S.J., Brown, P.D., Iacono, M.J. and Clough, S.A. (1997) Radiative transfer for inhomogeneous atmospheres: RRTM, a validated correlated-k model for the longwave. *Journal of Geophysical Research: Atmospheres*, 102(D14), 16663–16682. https://doi.org/10.1029/97JD00237.

Müller, G.V., Compagnucci, R., Nunez, M.N. and Salles, A. (2003) Surface circulation associated with frost in the wet pampas. *International Journal of Climatology*, 23(8), 943–961. https://doi.org/10.1002/joc.907.

Nishizawa, S., Yamaura, T. and Kajikawa, Y. (2021) Influence of sub-mesoscale topography on daytime precipitation associated with thermally driven local circulations over a mountainous region. *Journal of the Atmospheric Sciences*, 78(8), 2511–2532. https://doi.org/10.1175/JAS-D-20-0332.1.

Parise, C.K., Calliari, L.J. and Krusche, N. (2009) Extreme storm surges in the south of Brazil: atmospheric conditions and shore erosion. *Brazilian Journal of Oceanography*, 57(3), 175–188. https://doi.org/10.1590/S1679-87592009000300002.

Parise, C.K. and Farina, L. (2012) Ocean wave modes in the South Atlantic by a short-scale simulation. *Tellus A: Dynamic Meteorology and Oceanography*, 64(1), 17362. https://doi.org/10.3402/tellusa.v64i0.17362.

Pérez, J., Méndez, F.J., Menéndez, M. and Losada, I.J. (2014) ESTELA: a method for evaluating the source and travel time of the wave energy reaching a local area. *Ocean Dynamics*, 64(8), 1181–1191. https://doi.org/10.1007/s10236-014-0740-7.

Perez, J., Menendez, M., Camus, P., Mendez, F.J. and Losada, I.J. (2015) Statistical multi-model climate projections of surface ocean waves in Europe. *Ocean Modelling*, 96, 161–170. https://doi.org/10.1016/j.ocemod.2015.06.001.

Pezza, A.B. and Simmonds, I. (2005) The first South Atlantic hurricane: unprecedented blocking, low shear and climate change. *Geophysical Research Letters*, 32(15). https://doi.org/10.1029/2005GL023390.

Pryor, S.C. and Barthelmie, R.J. (2014) Hybrid downscaling of wind climates over the eastern USA. *Environmental Research Letters*, 9(2), 024013. https://doi.org/10.1088/1748-9326/9/2/024013.

Rao, V.B., Cavalcanti, I.F.A. and Hada, K. (1996) Annual variation of rainfall over Brazil and water vapor characteristics over South America. *Journal of Geophysical Research: Atmospheres*, 101(D21), 26539–26551. https://doi.org/10.1029/96JD01936.

Rao, V.B. and Hada, K. (1990) Characteristics of rainfall over Brazil: annual variations and connections with the Southern Oscillation. *Theoretical and Applied Climatology*, 42(2), 81–91. https://doi.org/10.1007/BF00868215.

Reboita, M.S., da Rocha, R.P., Ambrizzi, T. and Sugahara, S. (2010a) South Atlantic Ocean cyclogenesis climatology simulated by regional climate model (RegCM3). *Climate Dynamics*, 35(7–8), 1331–1347. https://doi.org/10.1007/s00382-009-0668-7.

Reboita, M.S., da Rocha, R.P., de Souza, M.R. and Llopart, M. (2018) Extratropical cyclones over the southwestern South Atlantic Ocean: HadGEM2-ES and RegCM4 projections. *International Journal of Climatology*, 38(6), 2866–2879. https://doi.org/10.1002/joc.5468.

Reboita, M.S., Gan, M.A., da Rocha, R.P. and Ambrizzi, T. (2010b) Precipitation regimes in South America: a bibliography review. *Revista Brasileira de Meteorologia*, 25(2), 185–204. https://doi.org/10.1590/S0102-77862010000200004.

Reynolds, R.W., Rayner, N.A., Smith, T.M., Stokes, D.C. and Wang, W. (2002) An improved in situ and satellite SST analysis for climate. *Journal of Climate*, 15(13), 1609–1625. https://doi.org/10.1175/1520-0442(2002)015<1609:AIISAS>2.0.CO;2.

Reynolds, R.W., Smith, T.M., Liu, C., Chelton, D.B., Casey, K.S. and Schlax, M.G. (2007) Daily high-resolution-blended analyses for sea surface temperature. *Journal of Climate*, 20(22), 5473–5496. https://doi.org/10.1175/2007JCLI1824.1.

Rueda, A., Cagigal, L., Antolínez, J.A.A., Albuquerque, J.C., Castanedo, S., Coco, G. and Méndez, F.J. (2019) Marine climate variability based on weather patterns for a complicated Island setting: the New Zealand case. *International Journal of Climatology*, 39(3), 1777–1786. https://doi.org/10.1002/joc.5912.

Rueda, A., Camus, P., Méndez, F.J., Tomás, A. and Luceño, A. (2016a) An extreme value model for maximum wave heights based on weather types. *Journal of Geophysical Research: Oceans*, 121(2), 1262–1273. https://doi.org/10.1002/2015JC010952.

Rueda, A., Camus, P., Tomás, A., Vitousek, S. and Méndez, F.J. (2016b) A multivariate extreme wave and storm surge climate emulator based on weather patterns. *Ocean Modelling*, 104, 242–251. https://doi.org/10.1016/j.ocemod.2016.06.008.

Saha, S., Moorthi, S., Wu, X., Wang, J., Nadiga, S., Tripp, P., Behringer, D., Hou, Y.-T., Chuang, H., Iredell, M., Ek, M., Meng, J., Yang, R., Mendez, M.P., van den Dool, H., Zhang, Q., Wang, W., Chen, M. and Becker, E. (2014) The NCEP Climate Forecast System version 2. *Journal of Climate*, 27(6), 2185–2208. https://doi.org/10.1175/JCLI-D-12-00823.1.

Salio, P. (2002) Chaco low-level jet events characterization during the austral summer season. *Journal of Geophysical Research*, 107(D24), 4816. https://doi.org/10.1029/2001JD001315.

Salio, P., Nicolini, M. and Zipser, E.J. (2007) Mesoscale convective systems over southeastern South America and their relationship with the south American low-level jet. *Monthly Weather Review*, 135(4), 1290–1309. https://doi.org/10.1175/MWR3305.1.

Seluchi, M.E. and Marengo, J.A. (2000) Tropical—Midlatitude exchange of air masses during summer and winter in South America: climatic aspects. *International Journal of Climatology*, 1190, 1167–1190. https://doi.org/10.1002/1097-0088(200008)20:10<1167::AID-JOC526>3.0.CO;2-T.

Seluchi, M.E., Saulo, A.C., Nicolini, M. and Satyamurty, P. (2003) The northwestern Argentinean low: a study of two typical events. *Monthly Weather Review*, 131(10), 2361–2378. https://doi.org/10.1175/1520-0493(2003)131<2361:TNALAS>2.0.CO;2.

Sheridan, S.C. (2002) The redevelopment of a weather-type classification scheme for North America. *International Journal of Climatology*, 22(1), 51–68. https://doi.org/10.1002/joc.709.

Short, A.D. and Klein, A.H.F. (2016) *Brazilian Beach Systems*. Cham: Springer.

Sillmann, J., Kharin, V.V., Zhang, X., Zwiers, F.W. and Bronaugh, D. (2013) Climate extremes indices in the CMIP5 multimodel ensemble: part 1. Model evaluation in the present climate. *Journal of Geophysical Research: Atmospheres*, 118(4), 1716–1733. https://doi.org/10.1002/jgrd.50203.

Silva Dias, M.A.F. and Jaschke, M.A. (1997) The role of local circulations in summertime convective development and nocturnal fog in São Paulo, Brazil. *Boundary-Layer Meteorology*, 82(1), 135–157. https://doi.org/10.1023/A:1000241602661.

Silva, V.B.S., Kousky, V.E. and Higgins, R.W. (2011) Daily precipitation statistics for South America: an intercomparison between NCEP reanalyses and observations. *Journal of Hydrometeorology*, 12(1), 101–117. https://doi.org/10.1175/2010JHM1303.1.

Smagorinsky, J. (1963) General circulation experiments with the primitive equations. *Monthly Weather Review*, 91(3), 99–164. https://doi.org/10.1175/1520-0493(1963)091<0099:GCEWTP>2.3.CO;2.

Solman, S.A. and Blázquez, J. (2019) Multiscale precipitation variability over South America: analysis of the added value of CORDEX RCM simulations. *Climate Dynamics*, 53(3–4), 1547–1565. https://doi.org/10.1007/s00382-019-04689-1.

Solman, S.A. and Menéndez, C.G. (2003) Weather regimes in the South American sector and neighbouring oceans during winter. *Climate Dynamics*, 21(1), 91–104. https://doi.org/10.1007/s00382-003-0320-x.

Sterl A. 2004. On the (in)homogeneity of reanalysis products. *Journal of Climate*, 17(19): 3866–3873. https://doi.org/10.1175/1520-0442(2004)017<3866:OTIORP>2.0.CO;2.

Stevaux, J.C., Latrubesse, E.M., Hermann, M.L.P. and Aquino, S. (2009) Floods in urban areas of Brazil. *Developments in Earth Surface Processes*, 13, 245–266.

Sun, F., Walton, D.B. and Hall, A. (2015) A hybrid dynamical–statistical downscaling technique. Part II: end-of-century warming projections predict a new climate state in the Los Angeles region. *Journal of Climate*, 28(12), 4618–4636. https://doi.org/10.1175/JCLI-D-14-00197.1.

Taylor, K.E. (2001) Summarizing multiple aspects of model performance in a single diagram. *Journal of Geophysical Research: Atmospheres*, 106(D7), 7183–7192. https://doi.org/10.1029/2000JD900719.

Tian, B., Fetzer, E.J., Kahn, B.H., Teixeira, J., Manning, E. and Hearty, T. (2013) Evaluating CMIP5 models using AIRS tropospheric air temperature and specific humidity climatology. *Journal of Geophysical Research: Atmospheres*, 118(1), 114–134. https://doi.org/10.1029/2012JD018607.

Trigo, R.M., Sousa, P.M., Pereira, M.G., Rasilla, D. and Gouveia, C.M. (2016) Modelling wildfire activity in Iberia with different atmospheric circulation weather types. *International Journal of Climatology*, 36(7), 2761–2778. https://doi.org/10.1002/joc.3749.

Walko, R.L. and Avissar, R. (2008a) The ocean–land–atmosphere model (OLAM). Part II: formulation and tests of the non-hydrostatic dynamic Core. *Monthly Weather Review*, 136(11), 4045–4062. https://doi.org/10.1175/2008MWR2523.1.

Walko, R.L. and Avissar, R. (2008b) The ocean–land–atmosphere model (OLAM). Part I: shallow-water tests. *Monthly Weather Review*, 136(11), 4033–4044. https://doi.org/10.1175/2008MWR2522.1.

Walko, R.L., Band, L.E., Baron, J., Kittel, T.G.F., Lammers, R., Lee, T.J., Ojima, D., Pielke, R.A., Taylor, C., Tague, C., Tremback, C.J. and Vidale, P.L. (2000) Coupled atmosphere–biophysics–hydrology models for environmental modeling.

Journal of Applied Meteorology, 39, 931–944. https://doi.org/10.1175/1520-0450(2000)039<0931:CABHMF>2.0.CO;2.

Walko, R.L., Cotton, W.R., Meyers, M.P. and Harrington, J.Y. (1995) New RAMS cloud microphysics parameterization. Part I: the single-moment scheme. *Atmospheric Research*, 38(1), 29–62. https://doi.org/10.1016/0169-8095(94)00087-T.

Walton, D.B., Sun, F., Hall, A. and Capps, S. (2015) A hybrid dynamical–statistical downscaling technique. Part I: development and validation of the technique. *Journal of Climate*, 28(12), 4597–4617. https://doi.org/10.1175/JCLI-D-14-00196.1.

Wenneker, I., Segal, A. and Wesseling, P. (2002) A Mach-uniform unstructured staggered grid method. *International Journal for Numerical Methods in Fluids*, 40(9), 1209–1235. https://doi.org/10.1002/fld.417.

Wilby, R.L., Charles, S.P., Zorita, E., Timbal, B., Whetton, P. & Mearns, L.O. Supporting material of the Intergovernmental Panel on Climate Change, available from the DDC of IPCC TGCIA

Wilby, R.L. and Wigley, T.M.L. (1997) Downscaling general circulation model output: a review of methods and limitations. *Progress in Physical Geography: Earth and Environment*, 21(4), 530–548. https://doi.org/10.1177/030913339702100403

World Bank. (2016) *Report of material damages and losses due to natural disasters in Brazil, 1995–2014*. Washington, DC: Centro Universitário de Estudos e Pesquisas sobre Desastres, World Bank.

SUPPORTING INFORMATION

Additional supporting information may be found in the online version of the article at the publisher's website.